doi.org/10.36721/PJPS.2026.39.2.REG.15152.1

An *in vitro* method to study pancreatic acinar cells and centroacinar cells: Co-culture of rat pancreatic acinar cells AR42J and human pancreatic ductal epithelial cells HPDE6-C7

Yifang Huo[1#], Huiying Yang[1,2,3#], Zhihai Liang[1], Yu Lei[1], Lianjie Lin[1] and Guodu Tang[1]*

[1]Department of Gastroenterology, The First Affiliated Hospital of Guangxi Medical University, Guangxi, China
[2]Key Laboratory of Early Prevention and Treatment for Regional High Frequency Tumor (Guangxi Medical University), Ministry of Education, Guangxi, China.
[3]Guangxi Key Laboratory of High-Incidence-Tumor Prevention & Treatment (Guangxi Medical University), Guangxi, China.

Abstract: **Background**: This study is aimed at creating a new co-culture model to study the interactions between centroacinar cells (CACs) and pancreatic acinar cells (PACs), as reliable in vitro systems to reproduce their *in vivo* interactions are limited. **Objective**: To create a reliable *in vitro* co-culture model to study CAC–PAC interactions in both healthy and pathological settings, utilizing human pancreatic ductal epithelial cells HPDE6-C7 and rat pancreatic acinar cells AR42J. **Methods**: AR42J cells were gradually acclimated to the growth conditions of HPDE6-C7 cells before co-culture. Caerulein (CAE) was used to cause acute pancreatitis (AP) in both co-cultured cells and rats. Brightfield microscopy was used to analyze co-cultured cells after pancreatic tissues were stained with hematoxylin and eosin. Using transmission electron microscopy (TEM), ultrastructural characteristics such as gap junctions (GJs) and tight junctions (TJs) were assessed and contrasted with *in vivo* PACs and CACs. Immunofluorescence was used to measure microfilaments (MF) and the TJ protein zonula occludens-1 (ZO-1). **Results**: Co-cultured cells showed normal morphology, and AR42J cells grew steadily during adaptation. TEM investigation revealed endoplasmic reticulum (ER) dilatation, nuclear condensation, and mitochondrial enlargement. While AR42J cells in the CAE group grew longer and took on a spindle-like form, HPDE6-C7 cells showed mitochondrial vacuolization. TJs and GJs were enlarged in both cell types, which is consistent with alterations seen in rat PACs and CACs. Immunofluorescence showed punctate MF distribution around AR42J nuclei and network-like MF structures in HPDE6-C7 cells, which is consistent with *in vivo* results. **Conclusion**: Co-culture model provides a reliable *in vitro* system for researching pancreatic cellular interactions and material exchange since it faithfully replicates PAC–CAC interactions seen *in vivo*.

Keywords: Centroacinar cells; Co-culture; Pancreatic acinar cells

Submitted on 05-09-2025 – Revised on 25-10-2025 – Accepted on 07-11-2025

INTRODUCTION

Acute pancreatitis (AP) is a common acute inflammatory disorder of the pancreas, characterized by sudden onset and rapid progression. In particular, severe acute pancreatitis (SAP) is associated with a high mortality rate (approximately 20%) (Mederos *et al*., 2021). Gallstones, alcoholism and hypertriglyceridemia are the most common causes of AP. These factors can induce abnormal pancreatic juice secretion or pancreatic structural damage, followed by premature activation of pancreatic enzymes in pancreatic acinar cells (PACs), ultimately triggering and exacerbating AP (Tenner *et al*., 2024; Lee & Papachristou, 2019; Sendler & Algül, 2021). Recent studies have confirmed that calcium overload in pancreatic cells, premature fusion of lysosomes with zymogen granules and organelle damage can result in abnormal pancreatic juice secretion (Sendler & Algul, 2021; Petersen *et al*., 2021; Saluja *et al*., 2019; Habtezion *et al*., 2019). Furthermore, impairment of the barrier function of pancreatic ductal epithelial cells (PDECs) is also a major contributor to the occurrence of AP (Yang *et al*., 2022). Therefore, a complete pancreatic structure, as well as unobstructed secretion and excretion of pancreatic juice, is key to preventing the occurrence of AP.

Under normal physiological conditions, pancreatic juice is mainly secreted by acinar cells of the exocrine pancreas, which serve as the storage site for zymogen granules. When food enters the gastrointestinal tract, a large number of zymogen granules are released from acinar cells. Together with water (H_2O) and bicarbonate (HCO^{3-}) secreted by PDECs, they form pancreatic juice. Centroacinar cells (CACs) are flat or cuboidal epithelial cells that extend into the pancreatic acinar lumen and are closely connected to acinar cells (Beer *et al*., 2016). They form the starting part of the pancreatic duct and participate together with acinar cells in the excretion of pancreatic juice. Pancreatic juice flows through the gaps between the CACs, converging into the elongated intercalated ducts. It then proceeds through the intralobular ducts, interlobular ducts and main pancreatic duct, ultimately being secreted into the intestine *via* the duodenal papilla to exert digestive functions (Gorelick *et al*., 2018). However, research on CACs remains scarce. The potential interaction

**Corresponding author:* e-mail: tangguodu@stu.gxmu.edu.cn
#Yifang Huo and Huiying Yang are co-first authors.

mechanisms between CACs and PACs remain unclear and their roles in the pathogenesis of AP or other pancreatic diseases are equally unknown. To address this bottleneck, this study presents a novel co-culture method involving rat pancreatic acinar cells (AR42J) and human pancreatic ductal epithelial cells (HPDE6-C7). This method can simulate the *in vivo* co-growth state of PACs and CACs, thereby offering new technical support for further investigations into the interaction mechanism between these two cell types.

MATERIALS AND METHODS

Animal model

Twelve 8-week-old specific-pathogen-free (SPF) male Sprague-Dawley rats, weighing 220-290 g, were randomly assigned to two groups: a control group (CG, n=6) and an AP group (APG, n=6). All animals were fasted for 12 hours before the experiment, with free access to water. The APG received intraperitoneal injections of caerulein (CAE; EY5113, Amquar, USA) at a dose of 50 μg/kg body weight per injection, administered once hourly for a total of seven injections. The CG was injected with an equal volume of normal saline *via* the same route. The rats were euthanized and dissected 24 hours after the final injection. All experimental procedures were approved by the Animal Ethics Committee of Guangxi Medical University (No: 202503010) and conducted in accordance with institutional and national guidelines for the care and use of laboratory animals.

Pancreatic histopathology

After collection of pancreatic tissues, the samples were fixed in 4% tissue fixative (P1110, Beijing Solarbio, China) and subsequently embedded in paraffin. The embedded tissues were sectioned into 4-μm-thick slices using a microtome, followed by hematoxylin-eosin (HE) staining. The sections were then observed under an upright microscope (Olympus Corporation).

Transmission electron microscope (TEM)

Rat pancreatic tissue (1 mm^3) and co-cultured cells were fixed separately: first with electron microscopy fixative (AFIHC 049, AiFang Biological, China) at 4°C for 2.5 hours, followed by 1% osmium tetroxide at room temperature for 2 hours. They were then dehydrated through a graded ethanol series and 100% acetone and embedded in a mixture of acetone and 812 embedding medium. Samples were sectioned into 60–80 nm slices using a microtome (Leica UC7), followed by counterstaining with 2% uranyl acetate and lead citrate for 15 minutes each. Images were acquired using a TEM (Thermo Fisher Scientific, Talos L120c).

Cell culture and treatment

Given that CACs are PDECs located within the pancreatic acinar lumen, the HPDE6-C7 and AR42J were selected to simulate the co-growth of CACs and PACs in this study. The HPDE6-C7 was obtained from WHELAB (https://www.whelab.com/pro/580.html; cat. no. C1248; passage 3), whereas the AR42J was purchased from the American Type Culture Collection (ATCC, Manassas, VA, USA). They were cultured in a thermostatic incubator maintained at 37°C with 5% CO_2 and 95% humidity. First, the culture conditions for HPDE6-C7 and AR42J cells were standardized prior to co-culture. The original culture conditions for AR42J cells were Ham's F-12K medium supplemented with 20% fetal bovine serum (FBS) and 1% penicillin-streptomycin. During medium replacement or subculture, the serum concentration was reduced by 2% each time and Ham's F-12K medium was gradually switched to DMEM in proportion (Ham's F-12K: DMEM = 9:1, 8:2, 7:3, 6:4, 5:5, 4:6, 3:7, 2:8, 1:9 and 0:10). When the cells were in good growth condition, the culture conditions for AR42J cells were adjusted to be consistent with those for HPDE6-C7 cells (DMEM supplemented with 10% FBS and 1% penicillin-streptomycin), which was referred to as standardized treatment. Subsequently, AR42J and HPDE6-C7 cells were then seeded into six-well plates at a cell count ratio of 8:2. Several proportions (5:5, 8:2 and 9:1) were tested in early optimization studies to determine this ratio. According to the *in vivo* acinar–ductal architecture, the 8:2 ratio consistently resulted in stable development, optimum co-culture morphology and distinct intercellular connection creation. When the co-cultured cells reached 60%–65% confluence, they were treated with CAE at a concentration of 10^{-7} mol/L for 24 hours and then divided into two groups: a CAE-treated group and a CG (cultured in CAE-free medium). The morphology and growth status of the co-cultured cells were observed using an inverted microscope (IX73, Olympus Corporation). Reproducibility and consistency of results were ensured by conducting all experiments in triplicate, with three distinct biological replicates (different passages of cells cultivated on various days) and three technical replicates per biological replicate. In order to make sure that the changes were caused by CAE alone and not by media adaption or cellular variations, more control groups were added. These included single-culture treatments, where each cell type (ductal or acinar) was cultivated independently and either treated with CAE or left untreated, as well as untreated co-cultures of AR42J and HPDE6-C7 cells kept under the same circumstances. Consistency was maintained by exposing all control groups to the same incubation times and medium modifications as the experimental groups.

Multiplex immunohistochemistry (mIHC)

Paraffin-embedded pancreatic tissue sections (4 μm) were deparaffinized with xylene and 100% ethanol, followed by rehydration with graded ethanol solutions. Heat-mediated antigen retrieval was performed using Tris-EDTA buffer (pH 8.0; AFIHC010, AiFang Biological, China). The sections were then blocked with 3% hydrogen peroxide for 15 minutes in the dark and subsequently with 10% normal goat serum (AFIHC011, AiFang Biological, China) for 30 minutes at room temperature. The sections were incubated

with primary antibodies, including carboxypeptidase (1:2000, AB278044, Abcam, UK), cytokeratin 19 (1:4000, AB52625, Abcam, UK) and Zonula Occludens-1 (ZO-1; 1:2000, 21773-1-AP, Proteintech Group, China) at 4°C overnight, followed by incubation with HRP-polymer anti-rabbit secondary antibody (AFIHC003, AiFang Biological, China) for 30 minutes at room temperature. Different tyramide-fluorophores (TYR-570, TYR-520, or TYR-650) were used to detect each primary antibody turn in, separating signals from the three antigens on the same tissue segment. Between staining sessions, the remaining HRP was deactivated to prevent cross-reactivity. The samples were stained with TYR-570, TYR-520, or TYR-650, respectively, for 5 minutes, followed by counterstaining with DAPI for 10 minutes. They were then mounted with an antifade mounting medium and observed under a fluorescence microscope.

Immunofluorescence staining of MF

The co-cultured cells were seeded onto round coverslips (24 mm in diameter) in six-well plates. When the cells reached 55%–60% confluence, they were fixed by immersion in 4% paraformaldehyde fixative solution (P1110, Beijing Solarbio, China) for 15 minutes at room temperature. Subsequently, the cells were permeabilized with 0.1% Triton X-100 (T8200, Beijing Solarbio, China) for 5 minutes. They were then stained with tetramethylrhodamine isothiocyanate-phalloidin (1:200, 500 μL/well, CA1610, Beijing Solarbio, China) for 30 minutes in the dark, followed by counterstaining with DAPI solution (ready-to-use, C0065, Beijing Solarbio, China) for 5 minutes in the dark. The samples were washed with PBS three times, with 5-minute intervals between each wash and mounted in anti-fading medium (S2100, Beijing Solarbio, China) in the dark. MF were visualized at 530–550 nm and cell nuclei were observed at 460–495 nm using an upright fluorescence microscope (Axio Imager A2; Carl Zeiss, Germany). For MF immunofluorescence staining of rat pancreatic tissue, we used fresh frozen sections. Prior to fixation, the sections were rewarmed in a 37°C oven for 15 minutes, with subsequent experimental steps identical to those for cell staining.

Immunofluorescence of ZO-1

The co-cultured cells were fixed with 4% paraformaldehyde fixative solution (P1110, Beijing Solarbio, China) for 15 minutes at room temperature, followed by blocking with 10% normal goat serum (SL038, Beijing Solarbio, China) for 30 minutes. Subsequently, the cells were incubated with the primary antibody against Zonula Occludens-1 (ZO-1; 1:500, 21773-1-AP, Proteintech Group, China) overnight at 4°C. The next day, the cells were incubated with an Alexa Fluor 488-conjugated secondary antibody (1:400, 550037, Chengdu Zen-Bioscience, China) for 1 hour at room temperature in the dark. The samples were washed with PBS three times, with 5-minute intervals between each wash, followed by counterstaining with DAPI solution (ready-to-use, C0065, Beijing Solarbio, China) for 5 minutes in the dark. Fluorescent images were captured using a fluorescence microscope (Axio Imager A2; Carl Zeiss, Germany).

Statistical analysis

All measurement data are expressed as mean ± standard deviation ($\bar{x} \pm s$). Statistical analyses were performed using SPSS 22.0 and graphs were generated with GraphPad Prism 5.0. For comparisons between two groups, homogeneity of variance was first tested. When $F > 0.05$ (indicating homogeneous variance), an independent samples *t*-test was used; $p < 0.05$ was considered statistically significant. For comparisons among three or more groups, homogeneity of variance was assessed *via* ANOVA ($F > 0.05$ indicating homogeneity). Homogeneous data were analyzed using one-way ANOVA with LSD post-hoc tests; heterogeneous data were corrected and compared using Dunnett's T3 method. $P < 0.05$ was considered statistically significant.

RESULTS

AR42J and HPDE6-C7 cells grew well in co-culture in vitro

AR42J cells exhibited a good growth state with little apoptosis under primary culture conditions (Ham's F-12K medium with 20% serum), appearing plump and forming clumps or clusters. AR42J cells grew well with a plump morphology and formed clumps or clusters as the serum concentration was gradually reduced. During each medium change or subculture, the serum concentration was reduced by 2% gradually until it reached 10% (Figs. 1A-B). When AR42J cells were directly cultured in DMEM medium (containing 10% serum), they became deformed, adopting a rod-like or spindle-shaped morphology and grew slowly. AR42J cells survived well as the culture medium was proportionally replaced with DMEM. During each medium change or subculture, the proportion of Ham's F-12K medium was reduced by 1% while that of DMEM was increased by 1%, until Ham's F-12K medium was completely replaced with DMEM (Figs. 2A-B).

AR42J and HPDE6-C7 cells grew well in co-culture. From 6 h through 12, 24 and 48 h, an increasing number of co-cultured cells and intercellular junctions between the two cell types were observed (Figs. 3A-C). The co-culture system's reproducibility was confirmed by the consistent observation of marker expression patterns and the creation of intercellular connections across three separate biological replicates, each with three technical replicates. Under white light, AR42J cells appeared round, exhibited good refractivity and were smaller than HPDE6-C7 cells, whereas HPDE6-C7 cells were spindle-shaped with poor refractivity. Under fluorescence, the DAPI fluorescence intensity of AR42J cells was stronger than that of HPDE6-C7 cells.

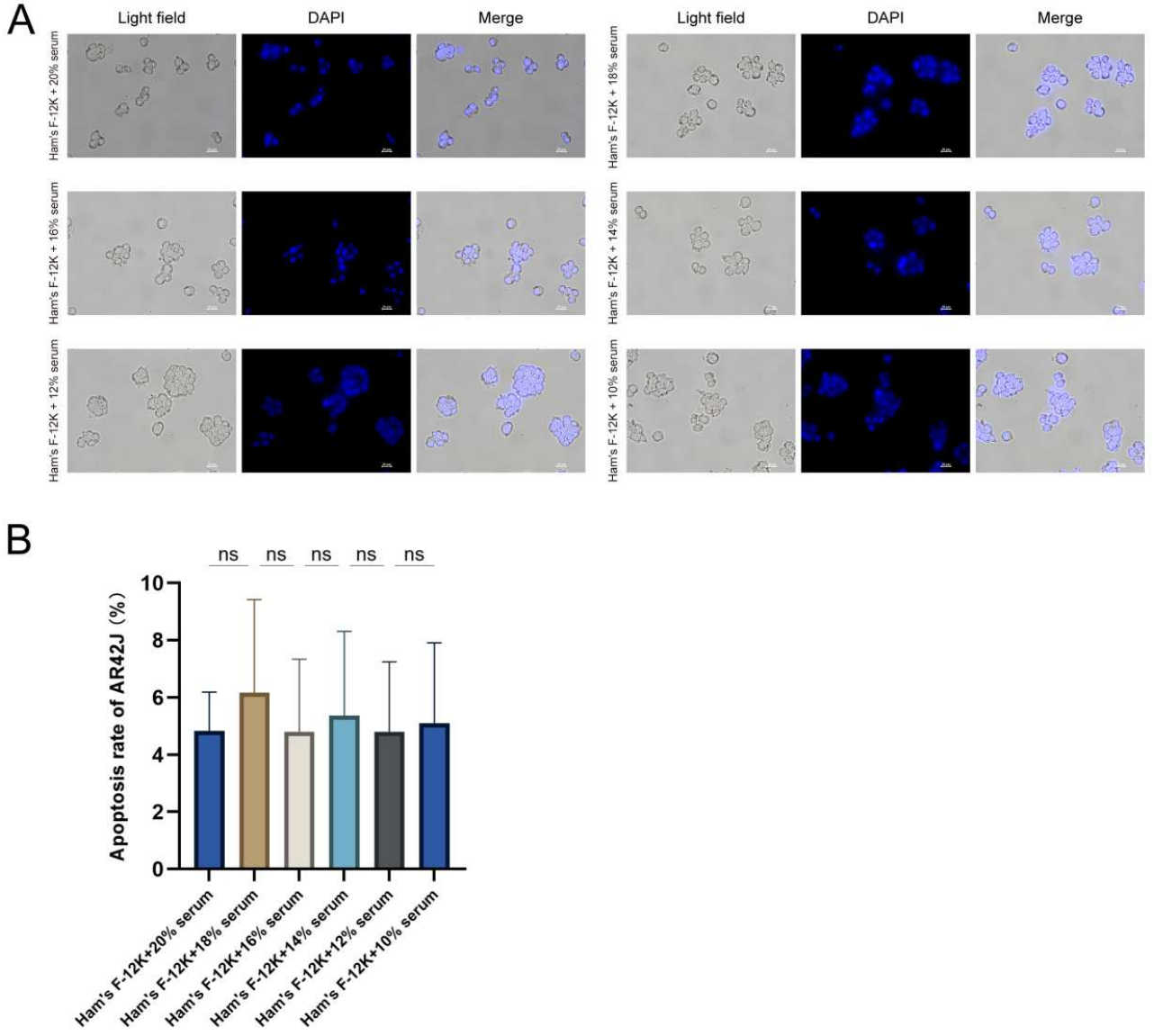

Fig. 1: AR42J cell growth during gradual serum replacement.
(A) Representative brightfield and DAPI images of AR42J cells cultured in Ham's F-12K medium with 20%,18%,16%,14%, 12%, and 10% serum (×400, scale bar = 20 μm). Cells maintained normal morphology across serum concentrations.
(B) Apoptosis rate of AR42J cells under different serum conditions (n = 3 independent experiments, mean ± SD). ns: no significance.

In vitro, changes in the ultrastructure and intercellular junctions of AR42J and HPDE6-C7 cells were consistent with the results of *in vivo* rat experiments.

In vitro, the co-cultured AR42J and HPDE6-C7 cells exhibited normal morphology and good growth status. After intervention with CAE, HPDE6-C7 cells maintained a morphology close to normal, while AR42J cells became elongated, thinner and even spindle-shaped by brightfield microscope (Fig. 4A). Other control groups were included to differentiate CAE-specific responses from baseline cellular behavior or medium adaption. These included single-culture treatments where each cell type was kept independently under the same culture conditions, as well as untreated co-cultures of AR42J and HPDE6-C7 cells. Throughout the observation period, untreated co-cultures and single-culture controls showed consistent morphology, distinct intercellular connections and low levels of apoptosis, demonstrating that CAE stimulation was the particular cause of the ensuing structural and inflammatory changes.

TEM showed that in the CAE group, AR42J cells exhibited nuclear condensation, mitochondrial swelling, endoplasmic reticulum dilation and an increase in fluid-filled vacuoles in the cytoplasm, while HPDE6-C7 cells showed slightly deeper nuclear staining, reduced cytoplasmic volume and increased mitochondrial vacuolation (Fig. 4B).

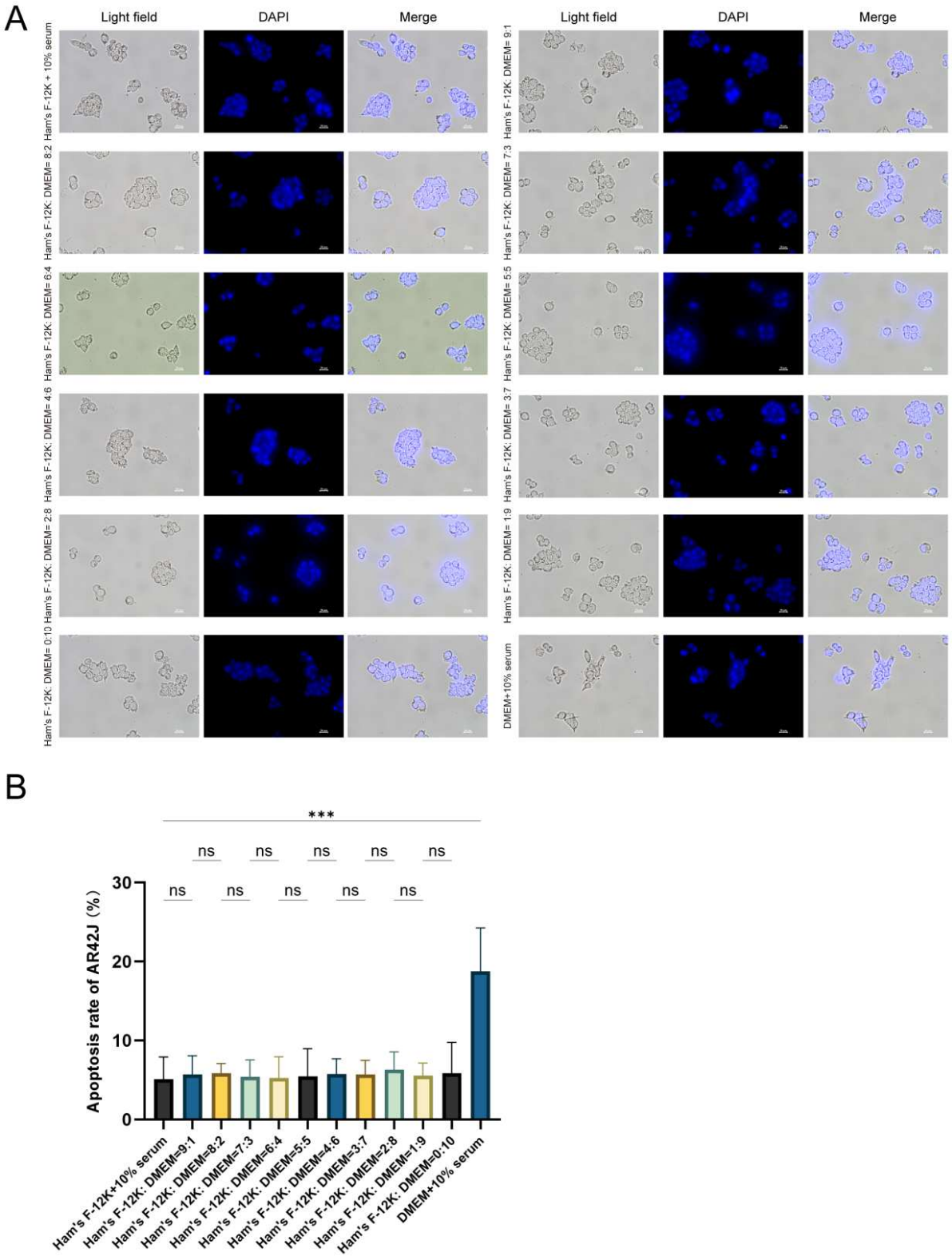

Fig. 2: AR42J cell viability during gradual replacement of the culture medium.
(A) Representative brightfield and DAPI images of AR42J cells cultured in Ham's F-12K : DMEM at ratios of 9:1, 8:2, 7:3, 6:4, 5:5, 4:6, 3:7, 2:8, 1:9, and 0:10 (×400, scale bar = 20 μm).
(B) Quantitative analysis of AR42J cell viability under different medium ratios (n = 3 independent experiments, mean ± SD). ***P < 0.001; ns: no significance.

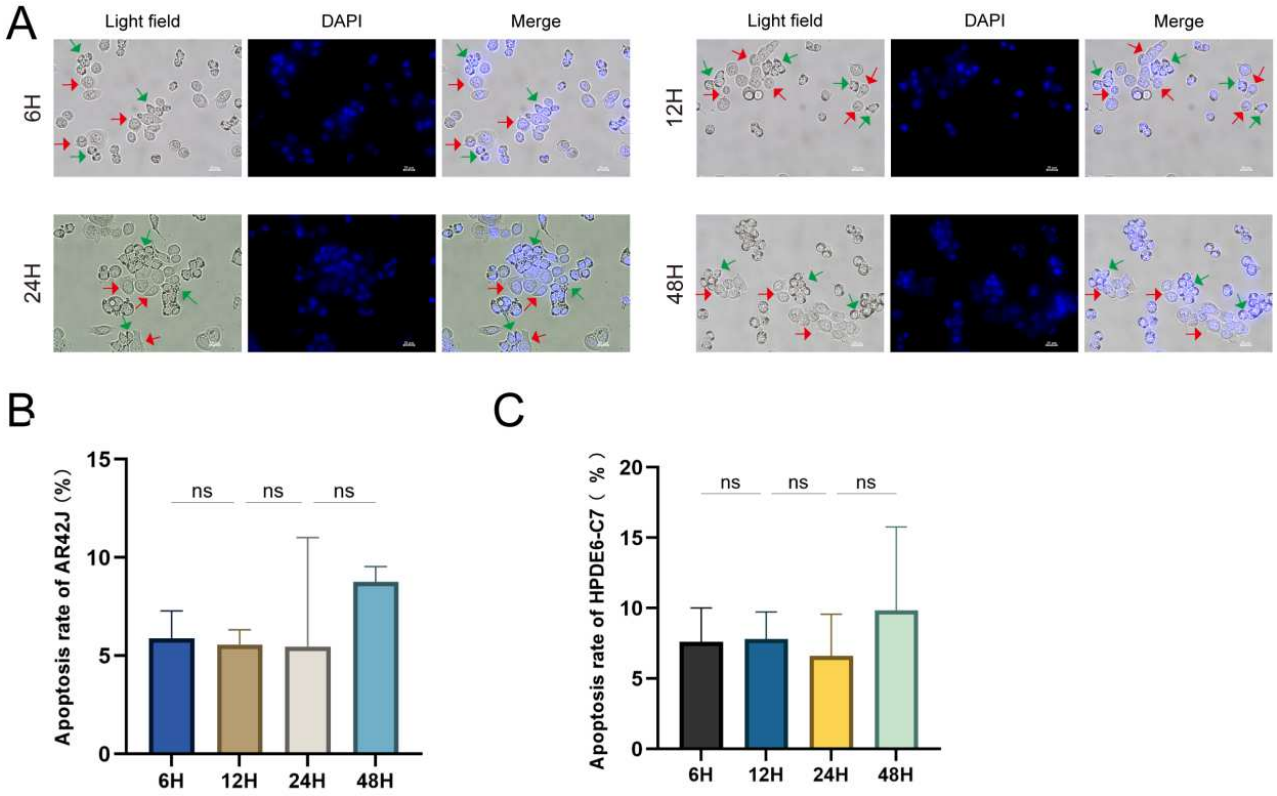

Fig. 3: Growth of AR42J and HPDE6-C7 cells in co-culture.
(A) Representative images showing the morphology of AR42J and HPDE6-C7 cells during co-culture at 6 h, 12h, 24 h, and 48 h (×400, scale bar = 20 μm). Green arrows indicate AR42J cells and red arrows indicate HPDE6-C7 cells.
(B) Quantitative comparison of co-culture viability (n = 3 independent experiments, mean ± SD). ns: no significance.

Meanwhile, in the CG, GJs and TJs could be observed between AR42J and HPDE6-C7 cells, whereas in the CAE group, these intercellular junctions became dilated (Fig. 4C). *In vivo*, PACs and CACs were visualized by HE staining. In the CG, CACs appeared as flat or cuboidal monolayer cells located within the acinar lumen. The nuclei of PACs were round and their cytoplasm was abundant. In the APG, CACs exhibited deformation and hyperchromatic nuclei. PACs were arranged in a disordered manner, with hyperchromatic nuclei, reduced cytoplasm volume and hypochromatic staining (Fig. 4D). TEM revealed that in the CG, the nuclei of CACs were round, with no mitochondrial deformation observed in the cells. For PACs, their nuclei were round and they had abundant cytoplasm containing a large number of endoplasmic reticula, mitochondria and zymogen granules. In the APG, CACs exhibited deformation, with condensed nuclei and vacuolated mitochondria. For PACs, their nuclei were condensed, with swollen and deformed mitochondria, increased and enlarged zymogen granules and expanded endoplasmic reticula (Fig. 4E). Meanwhile, we observed that both the TJs and GJs between PACs and CACs in the APG were wider than those in the CG (Figs. 4F-G). The results showed that the growth pattern of co-cultured AR42J and HPDE6-C7 cells was consistent with that of PACs and CACs *in vivo* and the changes between these two cell types after establishing the AP cell model using CAE were also consistent with those in the rat AP model. This indicates that the co-culture model can successfully simulate the *in vivo* conditions.

The fluorescent expression of MF in both in vitro and in vivo cells

In vitro, MF was observed between AR42J and HPDE6-C7 cells under a fluorescence microscope. Punctate microfilaments were observed surrounding the nucleus in AR42J cells, while MF with a regular network-like distribution was displayed in HPDE6-C7 cells (Fig. 5A). *In vivo*, MF were observed in both CACs and PACs. The MF of CACs appeared as strips surrounding the nucleus. Whereas the MF in the cytoplasm of PACs showed a punctate and filamentous distribution, with a strip-like arrangement along the cell membrane (Fig. 5B).

The fluorescent expression of ZO-1 in both in vitro and in vivo cells

In vitro, ZO-1 was observed between AR42J and HPDE6-C7 cells under a fluorescence microscope (Fig. 6A). *In vivo*, CACs were observed to localize at the center of the acinar lumen. Additionally, ZO-1 was detected between CACs and PACs (Fig. 6B).

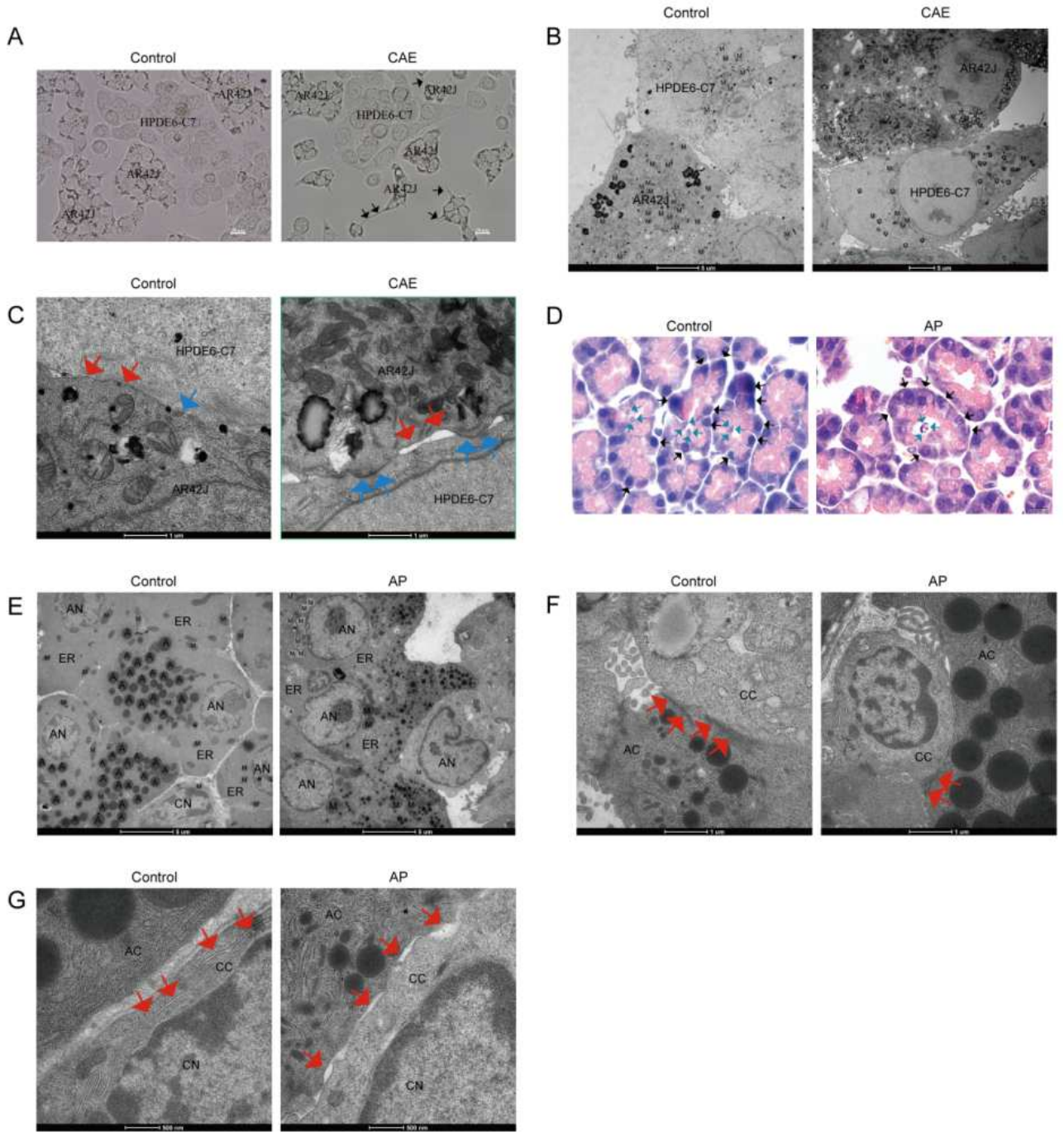

Fig. 4: Morphological comparison between *in vitro* and *in vivo* cells.
(A) Co-cultured HPDE6-C7 and AR42J cells observed under a brightfield microscope (×400; scale bar = 20 μm). Black arrows indicate deformed AR42J cells.
(B) Ultrastructure of co-cultured HPDE6-C7 and AR42J cells under TEM (×1250; scale bar = 5 μm).
(C) Intercellular GJs and TJs between co-cultured HPDE6-C7 and AR42J cells (×11,000; scale bar = 1 μm). Red arrows indicate GJs, blue arrows indicate TJs.
(D) PACs and CACs in CG and APG under HE staining (×1000; scale bar = 10 μm). Blue arrows = CACs; black arrows = PACs.
(E) Ultrastructure of PACs and CACs in CG and APG rats under TEM (×2600; scale bar = 5 μm). AN = acinar nuclei; CN = centroacinar nuclei; M = mitochondria; ER = endoplasmic reticulum; A = abundant zymogen secretory granules of varying size.
(F) TJs between PACs and CACs in CG and APG under TEM (×11,000; scale bar = 1 μm). Red arrows = TJs.
(G) GJs between PACs and CACs in CG and APG under TEM (×17,500; scale bar = 50 nm). Red arrows = GJs.
Note: N = nucleus; M = mitochondria; ER = endoplasmic reticulum; V = vacuole. (n = 3 independent experiments, mean ± SD)

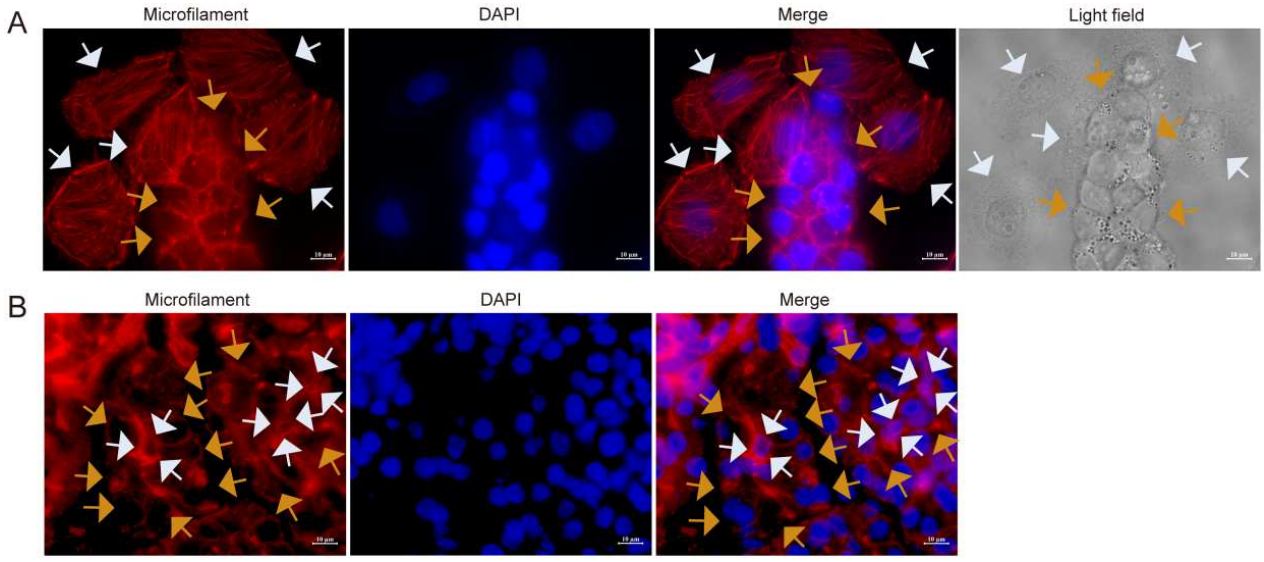

Fig. 5: Fluorescent expression of microfilaments (MF) in both *in vitro* and *in vivo* cells.
(A) MF distribution in AR42J and HPDE6-C7 cells. White arrows and orange arrows indicate HPDE6-C7 and AR42J cells, respectively (×1000, scale bar = 10 μm).
(B) MF expression in CACs and PACs from rat pancreatic tissue. White arrows and orange arrows indicate CACs and PACs, respectively (×1000, scale bar = 10 μm).
Note: Representative images from three independent experiments (n = 3).

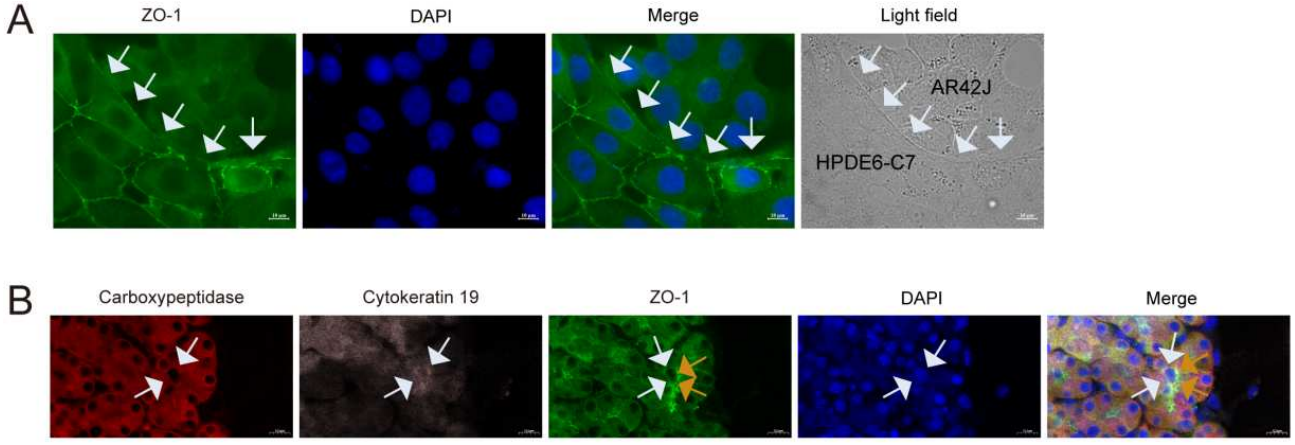

Fig. 6: Fluorescent expression of ZO-1 in both *in vitro* and *in vivo* cells.
(A) Localization of ZO-1 between AR42J and HPDE6-C7 cells in co-culture. White arrows indicate ZO-1 expression at intercellular junctions (×1000, scale bar = 10 μm).
(B) ZO-1 localization between CACs and PACs in rat pancreatic tissue. White arrows and orange arrows indicate CACs and ZO-1 expression, respectively (×800, scale bar = 12.5 μm).
Note: Representative images from three independent experiments (n = 3).

DISCUSSION

The exocrine pancreas is primarily composed of PDECs, PACs and CACs (Cleveland *et al*., 2012). Among these, CACs are flat or cuboidal in shape, smaller than PACs (with a diameter of less than 10 μm) and located in the central lumen of acini within the terminal ductal system (Williams & Kendall, 1982). They are involved in the secretion and excretion of pancreatic juice and play a crucial role in pancreatic exocrine function (Pallagi *et al*., 2015). Furthermore, CACs, as a crucial component of the blood-pancreas barrier (BPB), play a key role in maintaining pancreatic homeostasis and protecting acinar cells. In pancreatic pathological conditions, they also act as a barrier to drugs entering the pancreas, which is of great significance for the selection and optimization of therapeutic strategies (Wang *et al*., 2025; Hu *et al*., 2023).

Our study demonstrated that rat CACs were closely associated with PACs, with TJs and GJs present between

the two cell types. In the rat model of AP, CACs exhibited deformation and nuclei condensation, with vacuolated mitochondria; additionally, both TJs and GJs between CACs and PACs were dilated. These observations suggested that the interaction between CACs and PACs was involved in the pathogenesis of AP. Our mIHC experiments' use of sequential tyramide-based fluorophore labeling made it possible to distinguish precisely between carboxypeptidase, CK19 and ZO-1 signals within the same tissue section. This allowed for exact spatial observation of CACs and PACs as well as their interactions with other cells. Nevertheless, current research on *in vitro* studies of CACs primarily relied on the isolation and culture of primary cells (Mameishvili *et al*., 2019). Although primary cells can provide an experimental model that is closer to the *in vivo* environment, their complex isolation process, difficulty in ensuring cell purity, stringent requirements for culture conditions and the multiple factors influencing cell growth status and function make long-term culture challenging, which to some extent limits in-depth research on the functions of CACs. To address the aforementioned limitations and considering that CACs are a specialized type of ductal cell, this study is the first to establish an *in vitro* co-culture model using HPDE6-C7 and AR42J, aiming to simulate the interaction between CACs and PACs.

Given the differences in the culture conditions required for HPDE6-C7 and AR42J cells (Yang *et al*., 2022; Lei *et al*., 2024; Tang *et al*., 2017), standardizing the culture conditions for these two cell lines represented the primary breakthrough in this study. By replacing the culture medium of AR42J cells in specific proportions and gradually reducing the FBS content, we ultimately found that AR42J cells could also grow well under the same culture conditions as HPDE6-C7 cells. Consequently, these conditions were adopted for subsequent co-culture experiments. In this co-culture system of the two cell types, we also observed that both cells grew well, with TJs and GJs formed between them. This is consistent with the phenomenon observed in rat pancreatic tissue, indicating that the co-culture system can successfully simulate PACs and CACs *in vivo*. Thus, it provides a new approach for investigating the interaction mechanism between these two cell types. Our main goal was to create a trustworthy co-culture model of AR42J and HPDE6-C7 cells as a proof-of-concept investigation. Successful interactions between the two cell types were demonstrated by morphological evidence, such as cell survival, the creation of intercellular junctions and marker expression (microfilaments and ZO-1). Minimal evaluations, such as consistent junction formation and fluorescence patterns across three independent biological replicates with three technical replicates each, validated the co-culture system's stability and reproducibility even though in-depth quantitative analyses were not carried out at this time. This methodology guarantees the consistency of our observations and establishes a solid basis for subsequent mechanistic investigations.

CAE, an analog of cholecystokinin, has been extensively utilized in both *in vitro* and *in vivo* studies to induce AP models (Lerch & Gorelick, 2013). To further verify that the co-culture system of HPDE6-C7 and AR42J cells is applicable to *in vitro* research on pancreatic-related diseases, we induced an AP model in rats *via* intraperitoneal injection of CAE. It was observed that in the AP rat model, CACs exhibited mitochondrial vacuolation, while PACs showed microscopic changes including nuclear condensation, mitochondrial swelling and endoplasmic reticulum dilation. Additionally, the TJs and GJs between CACs and PACs were also found to be dilated. Subsequently, CAE was added to the HPDE6-C7 and AR42J co-culture system to establish an *in vitro* AP cell model. In this system, the microscopic structural changes of organelles in HPDE6-C7 and AR42J cells correspond respectively to those of CACs and PACs in the rat model. Previous studies *via* TEM revealed that *in vivo*, PDECs in AP-group rats exhibited nuclear condensation and deformation, along with mitochondrial vacuolation and swelling. *In vitro*, HPDE6-C7 cells in the CAE group also showed similar changes (Yang *et al*., 2023). Our findings were consistent with the above observations. Furthermore, the TJs and GJs between HPDE6-C7 and AR42J cells were also found to be wider accordingly. Previous studies demonstrated that TJs between HPDE6-C7 cells in the CAE group were wider than in the normal group by TEM (Yang *et al*., 2022; Wang *et al*., 2022). Our study showed that TJs between HPDE6-C7 and AR42J cells in the CAE group were also wider than in the normal group, which was consistent with their observations. This indicates that the HPDE6-C7/AR42J co-culture system can successfully simulate the *in vivo* state of CACs and PACs under disease conditions, providing a novel approach for pancreatic disease research. We included further control trials to be sure that the morphological and ultrastructural changes we saw were caused by CAE and not by variations in culture adaption or intrinsic diversity among cell types. These included untreated and CAE-treated single-culture treatments of AR42J or HPDE6-C7 cells, as well as untreated co-cultures of both cell types kept in the same environment. In contrast to the clear pathological alterations in the CAE-treated co-cultures, the control groups' constant morphology and junctional integrity demonstrated that the observed cellular responses were, in fact, CAE-specific. This increases our model's dependability and validates its applicability for *in vitro* simulation of CAE-induced pancreatic damage. While animal models can effectively simulate the pathogenesis of human diseases, they nonetheless have certain limitations. For example, while animal models allow visualization of cellular ultrastructures -including MF-*via* electron microscopy -they cannot capture their dynamic changes. Meanwhile, animal fluorescence staining has limitations:

the high cellular density in animal tissues makes it difficult to observe the MF cytoskeleton between two specific cells. In contrast, *in vitro* cell models can overcome these limitations and offer their own unique advantages, thereby laying a foundation for further mechanistic research.

While our research has provided a novel experimental approach for studying pancreatic diseases, it is not without limitations. Our study utilized direct co-culture of cell lines from different species. Further research is required to verify the discrepancies between this *in vitro* co-culture model and the actual *in vivo* growth of these cells in animals. In the next phase, we aim to conduct a more in-depth investigation into the mechanism by which this co-culture system functions in AP.

Acknowledgment
Not applicable.

Author's contributions
Yifang Huo and Huiying Yang contributed equally to this work. Yifang Huo and Huiying Yang designed and performed the experiments, analyzed the data and drafted the manuscript. Zhihai Liang and Yu Lei assisted in data collection and interpretation. Lianjie Lin contributed to statistical analysis and Fig. preparation. Guodu Tang supervised the project, reviewed and edited the manuscript and provided overall guidance. All authors read and approved the final manuscript.

Funding
This study was supported by the Guangxi Natural Science Foundation (Grant No. 2024GXNSFAA010406) and the National Natural Science Foundation of China (Grant No. 81970558).

Data availability statement
All data generated or analyzed during this study are included in this published article.

Ethical approval
All experimental procedures involving animals were reviewed and approved by the Animal Ethics Committee of Guangxi Medical University (Approval No. 202503010) and were conducted in accordance with national and institutional guidelines for the care and use of laboratory animals.

Conflict of interest
The authors declare that they have no conflicts of interest related to this work.

REFERENCES

Beer RL, Parsons MJ and Rovira M (2016). Centroacinar cells: At the center of pancreas regeneration. *Dev. Biol.*, **413**(1): 8-15.

Cleveland MH, Sawyer JM, Afelik S, Jensen J and Leach SD (2012). Exocrine ontogenies: On the development of pancreatic acinar, ductal and centroacinar cells. *Semin. Cell Dev. Biol.*, **23**(6): 711–719.

Gorelick FS, Pandol S and Jamieson JD (2018). Structure-function relationships in the pancreatic acinar cell. In: *Physiology of the Gastrointestinal Tract*, Academic Press, pp. 869–894.

Hu Q, Zhang S, Yang Y, Li J, Kang H, Tang W and Wan M (2023). Extracellular vesicle ITGAM and ITGB2 mediate severe acute pancreatitis-related acute lung injury. *ACS Nano*, **17**(8): 7562–7575.

Habtezion A, Gukovskaya AS and Pandol SJ (2019). Acute pancreatitis: A multifaceted set of organelle and cellular interactions. *Gastroenterology*, **156**(7): 1941–1950.

L Lee PJ and Papachristou GI (2019). New insights into acute pancreatitis. *Nat. Rev. Gastroenterol. Hepatol.*, **16**(8): 479–496.

Lei Y, Yang HY, Meng N, Qin YY, Xu MT, Xiang XL and Tang GD (2024). Mitochondrial calcium uniporter promotes mitophagy by regulating the PINK1/Parkin pathway in caerulein-treated pancreatic ductal epithelial cells in vitro. *Exp. Ther. Med.*, **27**(4): 147.

Lerch MM and Gorelick FS (2013). Models of acute and chronic pancreatitis. *Gastroenterology*, **144**(6): 1180–1193.

Mederos MA, Reber HA and Girgis MD (2021). Acute pancreatitis: A review. *JAMA*, **325**(4): 382–390.

Mameishvili E, Serafimidis I, Iwaszkiewicz S, Lesche M, Reinhardt S, Bölicke N and Gavalas A (2019). Aldh1b1 expression defines progenitor cells in the adult pancreas and is required for Kras-induced pancreatic cancer. *Proc. Natl. Acad. Sci. U.S.A.*, **116**(41): 20679–20688.

Pallagi P, Hegyi P and Rakonczay Z Jr (2015). The physiology and pathophysiology of pancreatic ductal secretion: The background for clinicians. *Pancreas*, **44**(8): 1211–1233.

Petersen OH, Gerasimenko JV, Gerasimenko OV, Gryshchenko O and Peng S (2021). The roles of calcium and ATP in the physiology and pathology of the exocrine pancreas. *Physiol. Rev.*, **101**(4): 1691–1744.

Sendler M and Algül H (2021). Pathogenesis der akuten Pankreatitis. *Der Internist*, **62**(10): 1034–1043.

Saluja A, Dudeja V, Dawra R and Sah RP (2019). Early intra-acinar events in the pathogenesis of pancreatitis. *Gastroenterology*, **156**(7): 1979–1993.

Tenner S, Vege SS, Sheth SG, Sauer B, Yang A, Conwell DL and Gardner TB (2024). American College of Gastroenterology guidelines: Management of acute pancreatitis. *Am. J. Gastroenterol.*, **119**(3): 419–437.

Tang X, Tang G, Liang Z, Qin M, Fang C and Zhang L (2017). Effects of ghrelin miRNA on inflammation and the calcium pathway in pancreatic acinar cells of acute pancreatitis. *Pancreas*, **46**(10): 1305–1313.

Wang D, Wang S, Liu J, Shi X, Xiong T, Li R and Ai K (2025). Nanomedicine penetrating the blood-pancreas

barrier for effective treatment of acute pancreatitis. *Adv. Sci.*, **12**(13): 2413925.

Wang J, Qin M, Wu Q, Yang H, Wei B, Xie J and Huang J (2022). Effects of lipolysis-stimulated lipoprotein receptor on tight junctions of pancreatic ductal epithelial cells in hypertriglyceridemic acute pancreatitis. *BioMed Res. Int.*, **2022**: 4234186.

Williams DW and Kendall MD (1982). The ultrastructure of the centroacinar cells within the pancreas of the starling (*Sturnus vulgaris*). *J. Anat.*, **135**(1): 173–180.

Yang HY, Liang ZH, Xie JL, Wu Q, Qin YY, Zhang SY and Tang GD (2022). Gelsolin impairs barrier function in pancreatic ductal epithelial cells by actin filament depolymerization in hypertriglyceridemia-induced pancreatitis in vitro. *Exp. Ther. Med.*, **23**(4): 1–10.

Yang H, Liang Z, Xie J, Wu Q, Qin Y, Zhang S and Tang G (2023). Gelsolin inhibits autophagy by regulating actin depolymerization in pancreatic ductal epithelial cells in acute pancreatitis. *Braz. J. Med. Biol. Res.*, **56**: e12279.